# Integrated Power Filters utlizing Skin- and Proximity Effect based Low-pass Interconnects

J.D. van Wyk jr.[1, #], W.A. Cronje[2, #], J.D. van Wyk[3, *]P.J Wolmarans[*], C.K. Campbell [♣]
# - Industrial Electronics Technology Research Group, Energy Lab, +27-11-489-2454
Rand Afrikaans University, P.O. Box 524, Auckland Park, Johannesburg, 2006, South Africa
* - Centre for Power Electronics Systems, Virginia Polytechnic and State University, Blacksburg, Virginia, 24061, USA
♣ - McMaster University, Ontario, Canada
dvw@ing.rau.ac.za , 2 – wacronje@ieee.org , 3 – daan@vt.edu

## Abstract

The necessity for low pass interconnects (LPI's) in future integrated power electronic modules is discussed. Utilization of the skin and proximity effect to realise such interconnects in stacked, planar form is proposed. Two types of LPI's, based on nominal current capacity, are synthesized, simulated, modelled and built. Good correlation between measured and calculated attenuation is obtained. Significant attenuation at HF, -40dB at 20MHz, is realised with a 11cm long structure. Nominal power frequencies pass unimpeded through the LPI. Influence of different parameters on LPI performance are investigated. Possible future work is discussed.

## 1 Introduction

Technologically, our world is progressing at a rate unknown in history. This rapid progress has ensured that parameters such as weight, volume and cost are more critical than ever during the development/design of any electrical energy processing product. It unfortunately also highlighted limitations in fossil fuel reserves, and increasing pollution levels, motivating generation with alternative means such as wind turbines, solar cells etc. Thus a situation exists where future power electronic systems will not only have to be cheaper, smaller, lighter etc., but will also be more abundant to ensure efficient distributed power generation. A modular integration philosophy for power electronic systems [1], is thus clearly merited.

But such possible future abundance also requires certain EMC levels, both within and between modules. Integration of low-pass filters into Integrated Power Electronic Modules (IPEM's) will therefore be critical to the successful implementation of a modular integration philosophy. Conventional discrete element LC low-pass filters can be realised in integrated form. One problem with this approach is the load conditionality of the filter response [2]. Another is the volume sacrificed within a module to realise a single function, that of filtering.

An interesting alternative is to integrate low-pass filters into IPEM interconnects, with increased high frequency dissipation to ensure lower load conditionality. Justification for this approach is three-fold. First, at present, interconnects are typically utilised for the singular function of guiding power between components, even within integrated systems. Such singular utilization is out of step with an integration philosophy. Secondly, interconnects are often the cause of generated EMI [3]. Incorporating low-pass filters along their length will ensure lower generated EMI levels. Thirdly, all conducted EMI propagates along interconnects. It is a logical step to make this propagation path as frequency selective as possible, significantly enhancing EMC in terms of susceptibility and generation.

However low-pass interconnects (LPI's) is not a new concept. Utilization of lossy ferrite's and the skin effect to realise low-pass coaxial cables has been reported in the literature for a few decades [4], [5]. Cables of this type are presently being used in aeronautical and military applications [6]. In microwave systems, many examples of the realization of interconnect based low-pass filters can be found [7], [8]. But LPI's are not common in power electronic systems, especially in planar, integrated form. We therefore investigated the possibility of integrated lossy low pass filters utilising stacked, multi-layered planar interconnects.

The biggest challenge with such lossy LPI's is to realise sufficient attenuation at unwanted high frequencies, without inhibiting power transfer at the nominal power processing frequency. Since the skin- and proximity effect typically affect higher frequencies more than nominal power frequencies, we based our investigation on utilization of these effects to overcome this challenge. It is envisaged, based on encouraging results obtained, that the proposed LPI technology become a generic technique for future integrated power electronic systems of varying power levels.

## 2 Conceptual Overview

The skin- and proximity effect govern all interconnect's high frequency current distribution. Figure 1 shows typical current distributions at low and high frequency for stacked planar conductors, with opposing current directions. The skin and proximity effects at high frequency (HF) are clear. Current crowding exists in peripheries and corners that are in close proximity. The hypothesis on which the LPI's are based, is that HF resistance can be significantly increased

through the introduction of low σ materials into area's of current crowding. This has been proved with the help with extensive FEM simulations, and measurements. A limitation in the amount of HF resistance possible, exist. If the σ becomes too low, or the area of low σ material too small, current will revert back to the low frequency path.

However, from the equation for attenuation realised by a transmissionline in (1), we can see that resistance is one of four parameters influencing attenuation.

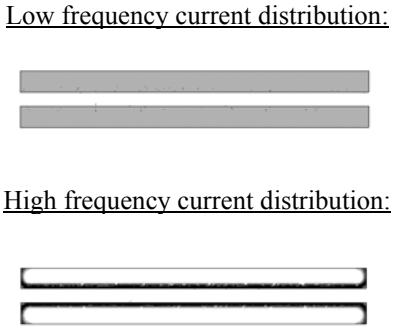


**Fig. 1:** Typical low and high frequency current distribution for stacked planar conductors.

$$\alpha = \mathrm{Re}(\gamma) = \mathrm{Re}\left(\sqrt{(R + j\omega L)(G + j\omega C)}\right) \quad [\mathrm{Np/m}] \qquad (1)$$

with R, L, G and C per meter values.

It can be shown with (1) that an increase in capacitance and conductance, and a decrease in inductance, in conjuction with significant HF resistance, leads to higher HF attenuation. To this end, we focussed on high permittivity $BaTiO_3$ based ceramics and location specific low σ materials, neglecting the influence of G and L at first.

# 3 LPI's Investigated:

LPI structures investigated can be split into two categories. The first consists of 10mm wide interconnects, with a copper thickness between 25 and 50μm, and a current capacity of 2.5 to 5A @10A/mm$^2$. Primary field of application for these interconnects at present is in IPEM's. High current planar busbars, with width of 50mm, copper thickness of 3mm, and capacity of 1500 A @ 10 A/mm$^2$, form the second category. These are investigated to determine the feasibility of LPI's at higher current levels in anticipation of future integration of high power converters, and for possible application to present industrial interference problems.

If we refer to Figure 1, a logical placement of low σ material will be in those regions of current crowding at HF, as Figure 2 illustrates. Since current crowding is more extensive in the corners facing one another, more HF resistance could be realised by decreasing the width of low σ "arms", as Figure 3 illustrates. But this decrease in width brings about lower capacitance, resulting in less HF attenuation. Therefore, a trade-off exists. The LPI resistance can be further increased through introduction of ferrite slabs to ensure flux cutting of low σ material at HF, as in Figure 3, increasing the trade-off complexity.

Due to the above mentioned trade-off, a large number of variations on Fig.'s 2 and 3 were investigated with FEM simulations, [9], [10], [11]. From these, an optimum structure for further investigation was identified, shown in Figure 4, named Design 17.

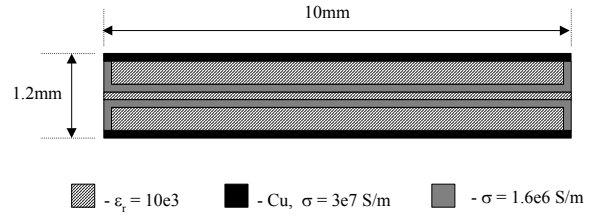


**Fig. 2:** Cross-section of possible LPI structure based on HF current distribution in Figure 1

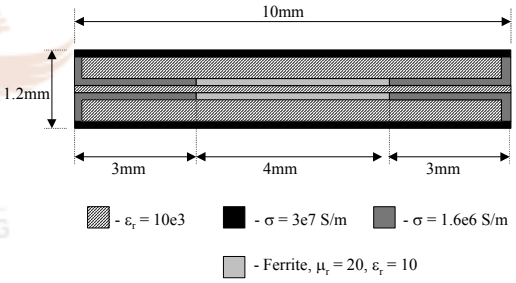


**Fig. 3:** Cross-section of LPI structure with shorter low σ arms, and ferrite slabs to increase HF resistance.

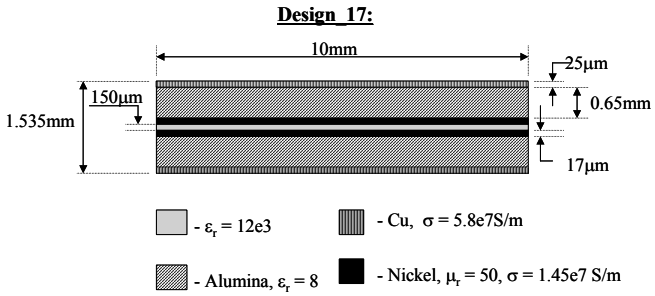


**Fig.4:** Cross section of Design 17, actual 10mm wide LPI investigated

As can be seen in Figure 4, no low σ material are present on the outer vertical edges of the alumina. This is done to ease manufacturing complexity. To maintain galvanic connection between the outer copper conductors, and the inner nickel conductors, the ends are connected in parallel, as shown in Figure 5.

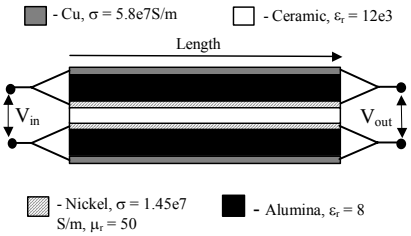


**Fig. 5:** Longitudal view of Design 17 showing connection of inner and outer lines.

The 50mm wide, high current busbars are based on the same geometries as the 10mm structures. Figure 6 illustrate a typical busbar, which realised 2.261Ω/m and 9.93dB/m at 100 MHz, compared to 229μΩ/m and 1.91e-5 dB/m at 1Hz, according to FEM simulations.

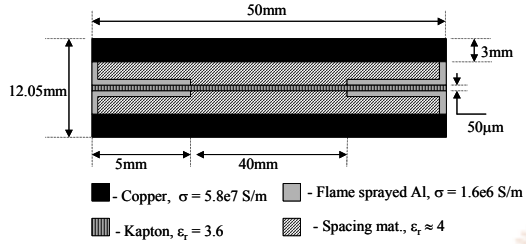


**Fig. 6:** Cross section of typical high current busbar LPI

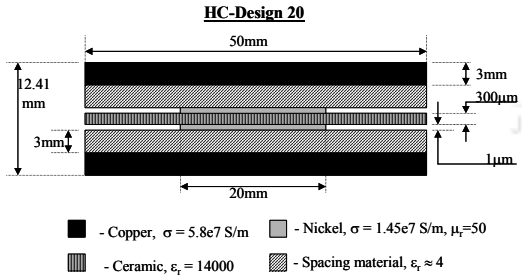


**Fig. 7:** Cross section of HC-Design20, actual 50mm wide, high current LPI investigated

The low value of HF attenuation for Fig. 6 is attributable to the dielectric $\varepsilon_r$ of 3.6. The low σ material utilised, with conductivity of 1e6 S/m [12], is flame sprayed aluminium. This material facilitates manufacture of the L-shaped low σ arms more easily. However, due to the low 100MHz attenuation, it was decided to utilise the same high permittivity ceramics as for the 10mm wide LPI's. Unfortunately, adhesion of flame sprayed aluminium to these tiles is poor. This has led to the use of Nickel as low σ material for the high current LPI's. Although a number of high current LPI's related to Fig. 6 have been evaluated with FEM, these will be not be discussed due to space constraints. Fig. 7 illustrates the high current LPI investigated. Named HC-Design20, it is closely related to Fig. 4, with differing dimensions and spacing material other than alumina being the main distinctions. The inner nickel line, and outer copper bars of HC-Desgin 20 is connected in the same manner as in Fig. 5.

Comparing Fig.'s 4 and 7, we see that 1μm Nickel is uilised for HC-Design 20, unlike the 17μm of Design 17. Such a thin conductor is impractical in terms of current density, especially if we consider the nominal copper current to be 1.5kA at 10A/mm$^2$. This thickness came about due to technical difficulties in realising thicker layers, since Design 17 and HC-Design 20 were manufactured at different locations. But utilising the 1μm thick Nickel does allow us to verify our analytical calculations. Realization of thicker layers are being investigated. Lengths for Design 17 and HC-Design20 were 0.13m and 0.11m respectively. These lengths arise from IPEM specifications, and sizes of ceramic tiles available

# 4 FEM Analysis:

A 2D FEM field solver package was utilised. As such, wavelength effects were neglected during the FEM analysis. To find resistance and inductance per unit length, eddy current analysis were performed, with electrostatic analysis done to find capacitance per unit length. Simulations were performed for frequencies between 20Hz and 50MHz. Table 1 lists the calculated per unit length parameters for Design 17 (Fig. 4). Due to excessive required computational capacity, which results from the large difference in conductor thicknesses, simulations for HC-Design20 could not be performed.

**Table 1:** FEM calculated L,C,R values for Design 17

| Design 17: | | | | |
|---|---|---|---|---|
| Capacitance per metre: | | 7.083 uF/m | | |
| Frequency: | R/m: | R/0.13m: | L/m: | L/0.13m: |
| [Hz] | [Ohm/m] | [Ohm] | [nH/m] | [nH] |
| 20 | 0.1173 | 0.0152 | 227.8 | 29.61 |
| 1.00E+03 | 0.1173 | 0.0152 | 227.8 | 29.61 |
| 1.00E+04 | 0.1173 | 0.0152 | 227.63 | 29.6 |
| 1.00E+05 | 0.1331 | 0.0173 | 211.3 | 27.5 |
| 1.00E+06 | 0.5895 | 0.0766 | 57.4 | 7.46 |
| 1.00E+07 | 1.935 | 0.2516 | 35.7 | 4.64 |
| 5.00E+07 | 4.6487 | 0.6043 | 25.88 | 3.36 |

From the values in Table 1, it is clear that LPI resistance increase at a high rate above 1MHz, and inductance decrease significantly, as the current starts to flow in the inner line. Neglecting the conductance, we can calculate the LPI frequency dependent attenuation with (1). To find input voltage attenuation in dB/m from Np/m, we multiply by a factor of 8.683 [13]. Figure 8 illustrates the FEM based attenuation of Design 17, vs. frequency. It is clear that Design 17 realises significant attenuation , with the –3dB point situated around 1MHz.

Figures 9 and 10 show FEM current density plots for Design 17 at 20Hz and 50MHz respectively. The current density at 50MHz is only shown for the Ni conductors, since virtually no current flows in the outer Cu conductors. It should also be noted that current at 50MHz flows in a skin much thinner than the 17μm thickness of the Nickel conductors. At 50 MHz, the skin depth for Ni is 2.6 μm,

which is very close to the current layer thickness displayed in Fig. 10.

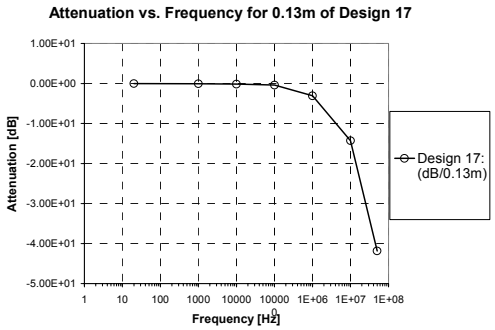


**Fig. 8:** Attenuation as calculated from FEM results.

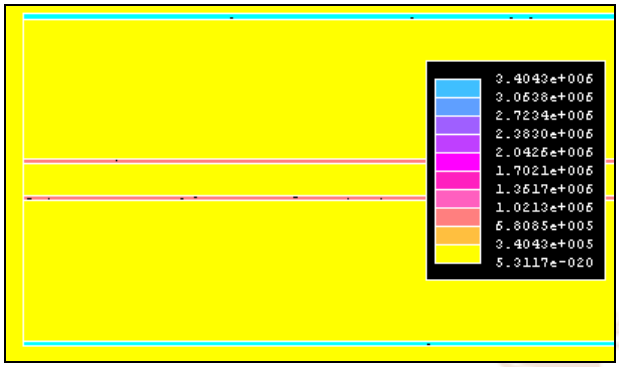

**Fig. 9:** FEM current density for Design 17 at 20Hz

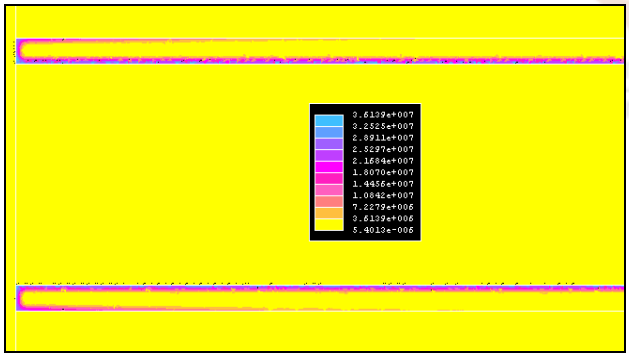

**Fig. 10:** FEM current density for inner Ni conductors of Design 17 at 50 MHz.

# 5 Analytical Model:

The analytical model is based on lossy transmissionline equations, taking additional losses due to the skin effect directly into account, and indirectly those due to the proximity effect. It approximates the LPI's as multiple, parallel connected lossy lines, and neglects capacitance and conductance due to the spacing material between the high and low σ layers. MathCad is utilised to implement the model.

First the skin depths δ for Nickel and Copper as a function of frequency are calculated with (2).

$$\delta = \sqrt{\frac{1}{\pi f \mu \sigma}} \quad [\text{m}] \qquad (2)$$

Next an effective conductor thickness $t_{eff}$ is defined for Copper and Nickel with the help of an if statement, as in (3).

$$t_{eff} = \text{if}\,(\delta \le \text{metal thickness}, \delta, \text{metal thickness}) \qquad (3)$$

The above statement reads: if the skin depth δ is smaller or equal to the metal thickness, the effective thickness is δ, otherwise it is the metal thickness. Utilsing this statement, it is possible to define a general, frequency dependent resistance per unit length, for all frequencies, as in (4). This approximation also incorporates the proximity effect indirectly, as Figure 10 shows.

$$R_{interconnect}/m = \frac{2}{t_{eff} * width * \sigma} \quad [\Omega/\text{m}] \qquad (4)$$

Equation (4) is valid, since the width of the conductors is much greater than their thickness in both the 10mm and 50mm width cases, and due to the proximity effect. If the thickness becomes an appreciable part of the width, current will not flow in a single layer, but all around the periphery. The factor 2 in (4) reflects the fact that the LPI consists of input and return conductors. Next we define the inductance of the interconnects, as in (5) to (7), from [14]

$$L_{total} = F_{skin} * L_{internal} + L_{external} \quad [\text{H/m}] \qquad (5)$$

$$L_{external} = \mu_0 \frac{conductor\_spacing}{width} \quad [\text{H/m}] \qquad (6)$$

$$L_{internal} = \mu \frac{2 * metal\_thickness}{3 * width} \quad [\text{H/m}] \qquad (7)$$

For the nickel conductors, the conductor spacing is the ceramic thickness. For the copper conductors, it is the sum of the ceramic thickness and twice the alumina thickness (neglecting the nickel thickness). The skin-effect factor $F_{skin}$ in (5) compensates for the fall-off in internal inductance with frequency, and is defined in (8).

$$F_{skin} = if\left(\delta < metal\_thickness, \exp\left(1 - \frac{metal\_thickness}{\delta}\right), 1\right) \qquad (8)$$

Next we define the series impedance of the Nickel and Copper conductors as:

$$Z_{interconnect} = R_{interconnect} + j2\pi f L_{total} \quad [\Omega/\text{m}] \qquad (9)$$

Since the Nickel and Copper conductors are connected in parallel, as in Fig. 5, we can define a parallel combination of their series impedances.

$$Z_{parallel} = \frac{Z_{Cu} * Z_{Ni}}{Z_{Cu} + Z_{Ni}} \quad [\Omega/\text{m}] \qquad (10)$$

Since the HF current distribution between the parallel inner and outer lines are determined by the impedance of the two

lines, (10) further incorporates the proximity effect, although indirectly. Distributed capacitance realised by the LPI's can be calculated with (11) , [14].

$$C_{\text{int}erconnect} = \frac{\varepsilon_0 \varepsilon_r * width}{ceramic\_thickness} \quad [\text{F/m}] \qquad (11)$$

Equation (11) neglects the capacitance due to other dielectrics in the LPI. Next we find the conductance of the LPI with (12), [14], once again neglecting all dielectrics except the high permittivity ceramic tile.

$$G_{\text{int}erconnect} = 2\pi f \varepsilon_0 \varepsilon_r \tan\_delta\left(\frac{width}{ceramic\_thickness}\right) \quad [\text{S/m}] \qquad (12)$$

From equations (10), (11) and (12), we can find the characteristic impedance of the LPI with (13).

$$Z_0 = \sqrt{\frac{Z_{parallel}}{G_{\text{int}erconnect} + 2\pi f C_{\text{int}erconnect}}} \quad [\Omega] \qquad (13)$$

To find the voltage attenuation in dB, we utilise equations (14) and (16), from [15], with the propagation constant γ in (14) defined by (15). The variable *l* in (14) is the LPI length.

$$V_{TRANSFER} = \frac{V_{out}}{V_{in}} = \frac{1}{\left[\cosh(-l*\gamma) - \frac{Z_0}{R_{load}}\sinh(-l*\gamma)\right]} \qquad (14)$$

$$\gamma = \sqrt{\left(G_{\text{int}erconnect} + j2\pi f C_{\text{int}erconnect}\right) * \left(Z_{parallel}\right)} \qquad (15)$$

$$Attenuatio\, n_{Voltage} = 20\log\left(\left|V_{TRANSFER}\right|\right) \qquad (16)$$

To find the phase reponse of the LPI, we once again utilise an if statement, as in (18). Equation (17) defines the phase response of the LPI's.

$$Phase = a\tan\left(\frac{\text{Im}(V_{TRANSFER})}{\text{Re}(V_{TRANSFER})}\right) * \frac{180}{\pi} \quad [\text{Deg}] \qquad (17)$$

$$Phase = if\left[\left(\text{Im}(V_{TRANSFER}) < 0\right) \cdot \left(\text{Re}(V_{TRANSFER}) < 0\right), -\left(180 - |Phase|\right), Phase\right] \quad [\text{Deg}] \qquad (18)$$

Utilising the above analytical model, voltage attenuation and phase response curves for 0.13m of Design 17 (Fig. 4) and 0.11m of HC-Design 20 (Fig. 7) were calculated. Figures 11 to 14 respectively illustrates the calculated curves.

Considering the attenuation curve in Fig. 11, we see that it has a flat response up to 400kHz, after which a series resonant peak occurs followed by an increase in attenuation above 10MHz of approximately 50dB/decade. This is higher than the –40dB/decade of a second order low-pass filter. Thus, low frequencies pass unimpeded, and frequencies above 10MHz are attenuated significantly.

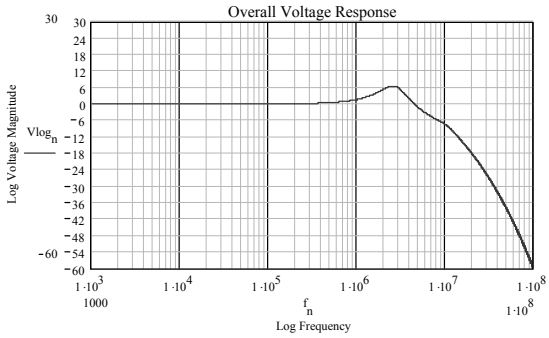


**Fig. 11:**Analytically calculated voltage response for Design 17.

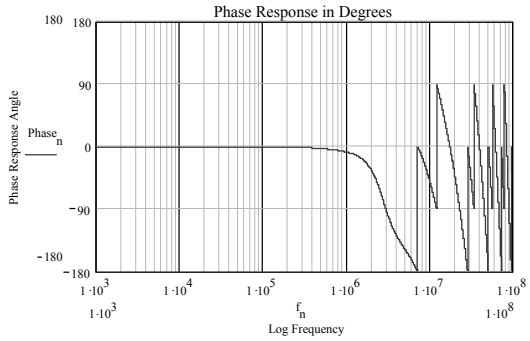


**Fig. 12:** Analytically calculated phase reponse for Design 17.

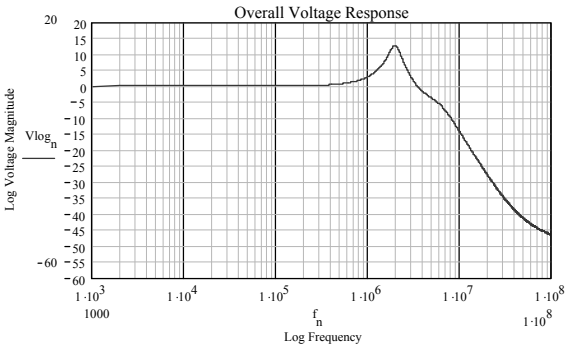


**Fig. 13:** Analytically calculated voltage reponse for HC-Design 20.

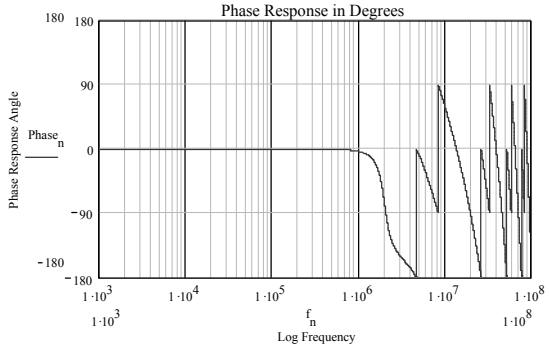


**Fig. 14:** Analytically calculated phase response for HC-Design 20.

Fig. 11 is also very similar to the FEM based results in Fig. 8. The main distinctions are the series resonant peak of +6dB at 2.5MHz in Figure 11, and the drop-off point in Figure 8 which lies at approximately 100kHz, as opposed to Figure 11's gain increase which starts at 400kHz. Since the FEM result is for a 2D plane, it can be expected that wavelength effects will not be present. Considering the phase response in fig. 12, we observe a zero degrees phase shift up to approximately 1MHz., with phase swings between +90° and -180° beyond 1MHz. The zero degree shift up to 1MHz is a desired result, assuring unaltered low frequency propagation.

From Fig. 13, it is clear that HC-Design 20 also realises significant attenuation above 1MHz. It's 100MHz value of –46 dB translates to –418dB/m, which is much higher than the –9.93dB/m realised by the structure in Figure 6. The series resonant peak, at +12dB, is higher than in Fig. 11, and occurs at lower frequency. If we increase the Nickel thickness to 5µm, we get a response as in Figure 15, with a smaller peak, but also less attenuation. Significantly higher attenuation of HC-Design20 is possible through an increase in length. Since length is at less of a premium for high current busbars than IPEM's, this will be adressed in Section VII, dealing with parametric analysis.

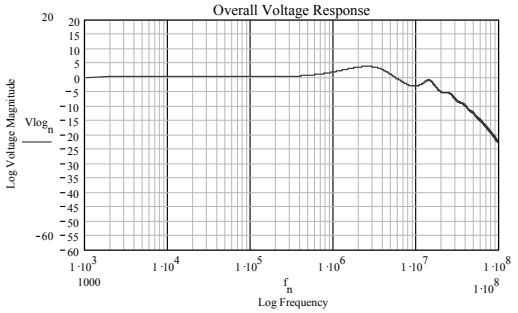


**Fig. 15:** Attenuation response obtained if Ni thickness is increased to 5µm.

# 6 Experimental Results:

Design 17 was manufactured in a 50mm x 50mm x 50mm U-shape, as required for integration into IPEM's [16]. For details of the construction process, refer to [16]. Figure 16 shows a photograph of the filter structure. HC-Design 20 was manufactured with a 20mm wide, 110mm long tile, and is shown in Figure 17.

Gain/phase measurements were taken with an HP3577B Network Analyzer. Considerable care was taken to ensure that BNC-connections between the coax measurement cables and the filter structures introduce minimal additional inductance. This can be seen in Figure 18, which shows a typical measurement setup. Measured gain/phase for Design 17 and HC-Design 20 are shown in Figures 19 and 20 respectively.

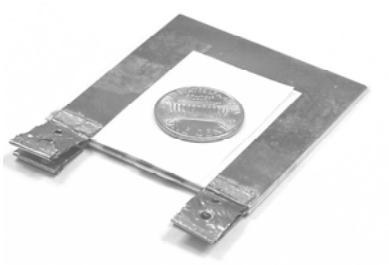


**Fig. 16:** Physical structure of Design 17 investigated.

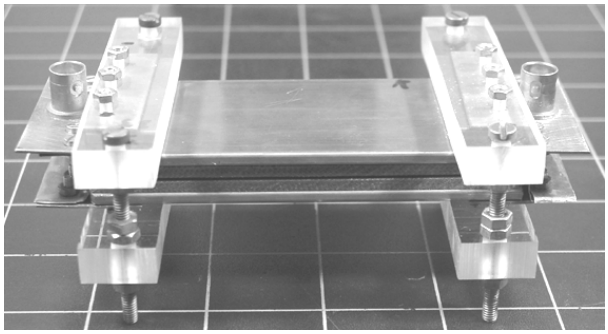

**Fig. 17:** Physical structure of HC-Design 20 investigated

**Fig. 18:** Typical coax to filter connections, with BNC connectors, and as small loop as possible.

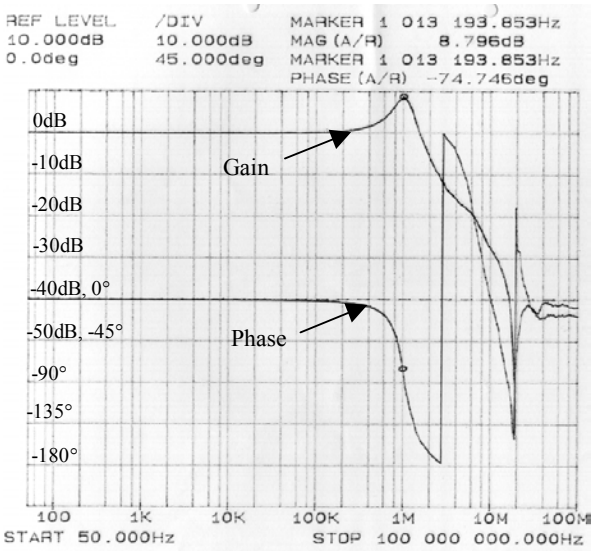


**Fig. 19:** Measured gain/phase curve for 0.13m of Design 17.

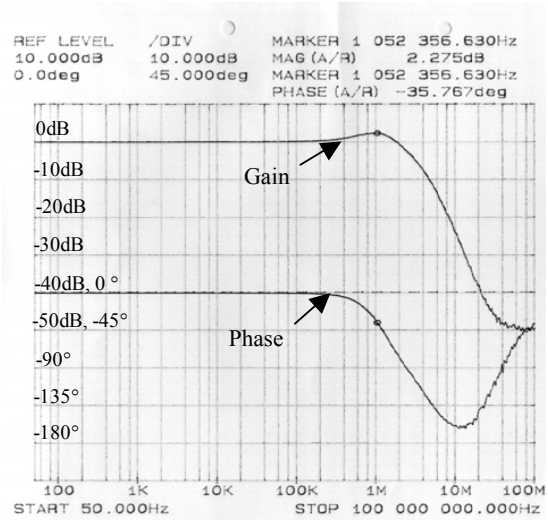


**Fig. 20:** Measured gain/phase curve for 0.11m of HC-Design 20.

Comparing Fig. 19 to Fig.'s 11 and 12, we find good correlation between the analytically calculated and measured responses. The biggest difference exists in the peak/drop-off frequencies. In Figure 19, the peak occurs at 1MHz, whilst it is calculated 1.5MHz higher, at 2.5MHz. Peak amplitude is measured as 8.7dB, versus a calculated value of 6dB. At 20MHz, attenuation is measured at approximately –40dB and calculated at –18dB. Phase response also differ slightly in frequency. Measured phase swing occurs between ±180 °, versus Fig. 12's -180° to 90° phase swing. Above 30MHz, it seems as if a measurement anomaly occurs, since both the phase and gain stays constant up to 100 MHz. A possibility is that the signal from the filter output is below the noise level of the Network Analyzer.

If we look at the measured and calculated gain/phase responses for HC-Design 20 in Fig.'s 20 , 13 and 14 respectively, fair correlation for the gain can be observed. The biggest difference lies in the series resonant peak amplitude, with +2dB measured and +12dB calculated. The peak frequency difference is 1MHz. Attenuation at 20MHz is measured at –40dB, and calculated at –30dB. Little correlation exist for the measured and calculated phase responses. The only similarity is the flat 0°phase reponse at low frequencies. The measured phase does swing down to –180° as expected, but not to +90°.

The cause of differences between measurments and calculations are being investigated. Possibilities are the proximity effect, which is only taken into account indirectly, and in the case of HC-Design 20, possible additional contact resistance between the inner and outer lines, due to manufacturing processes. It is also suspected that the metal deposition process utilised in the HC-Design 20 case resulted in an increase in conductance/ tan delta of the ceramic, due to nickel deposition within the ceramic.

LPI capacitance measurements were made with a HP 4284A LCR meter. This was done to verify relative permittivity values of the ceramics, and the analytical model assumption that the spacing material capacitance can be neglected. For Design 17, 6.942μF/m was measured, comparing well with the 7.083μF/m simulated and calculated. HC-Design 20 had a measured value of 8.728μF/m, close to the 8.26μF/m calculated.

# 7) Parametric Analysis:

Since correlation between the analytically predicted and the measured response of Design 17 is acceptable, the model of section V was utilised to determine the influence of different parameters on HF-attenuation. Although each parameter should be investigated for a range of values, only a few were covered, since overall gain/phase reponse curves need to be presented, and space is constrained. For all cases, parameters, except the parameter under investigation, were as described for Design 17 and HC-Design 20 in sections III. For instance, all cases investigating length, had loads of 50Ω (Network Analyzer), and all cases investigating different loads, had lengths of 0.13 or 0.11m.

Results of the parametric analysis are presented in Appendix A in graphical form. From these, we can highlight the following characteristics:

- Attenuation for both Design 17 and HC-Design 20 is proportional to length. In the case of HC-Design 20, Fig. A.19), a 0.5m long interconnect realise very high attenuation above 1MHz, although resonant effects are more dominant. Such a length is not impractical for 1500A nominal current interconnects.

- The frequency response of Design 17 is independent of load, for loads above 1Ω. Fig.'s A4 to A7 illustrate this characteristic. It can be explained from a charactersistic impedance viewpoint. Fig. 21 plots the characteristic impedance for Design 17. Above 1MHz, the characterisitic impedance is less than 0.2Ω. Any load larger than 1Ω thus appears as an open circuit, resulting in the same voltage response for all loads above 1Ω.

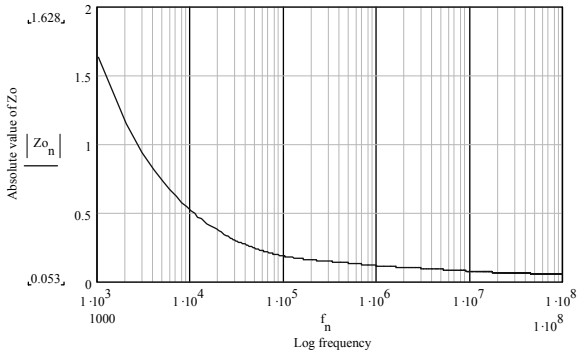


**Fig. 21:** Characteristic impedance of Design 17

- If we decrease the inner line's conductivity, higher values of HF attenuation is attainable. (Fig.'s A8 to A10) However, this is offset by larger resonant effects and a higher drop-off frequency. It can be qualitatively explained as follows. A lower inner line conductivity implies higher resistance. Thus the frequency at which current starts to flow in the inner line due to too high outer line impedance, increases. Since the effective resistance is thus lower at a given frequency, more resonant effects occur (Fig. A8). But once current does flow in the iner line, it's higher resistance ensures more attenuation.
- For relative permeability of 1, Design 17 realise very little HF attenuation, and more resonant effects occur (Fig. A11). An increase in permeability leads to more HF attenuation, but not resonant effects. Relative permeability of 600 gives attenuation for Design 17 closer to the measured curve. Since some material libraries [17] list this as Nickel's $\mu_r$, it could explain the difference between measurement and correlation.
- For Design 17, decreasing the relative permittivity of the ceramic to 500 leads to significantly lower HF attanuation, and a shift in the series resonant peak to 20MHz. An increase in relative permittivity leads to more HF attenuation, although the difference between $\varepsilon_r$ of $14*10^3$ and $20*10^3$ is not significant (Fig. A16).

# 8 Discussion and Conclusion

It was proposed and justified that LPI's become a generic technique in future integrated power electronic module technology. To this end, two LPI's, with respective nominal current capacities of 2.5 and 1500A at 10A/mm$^2$. and widths of 10mm and 50mm, were investigated. FEM simulations were utilised to identify feasible structures in the 10mm case. A first iteration analytical model, taking the skin effect directly, and the proximity effect indirectly, into account, was developed. Predicted voltage response from the analytical model correlate well with measurements. Fair phase correlation exist in the 10mm, but not for the 50mm case. The influence of various parameters on LPI response were investigated with the analytical model. From the parametric analysis, it was shown that the structures under consideration have frequency responses independent of load size, for loads above 1Ω.

The measured HF-attenuation realized by the LPI's synthesized, is significant. If we take the –40dB at 20MHz realized by both Design 17, and HC-Design 20, and translate it to per unit length, we obtain –307.7dB/m and –363dB/m respectively. Comparing these values with those quoted in [5], we find them significantly higher. The structures introduced/proposed also lends themselves more to integration technologies than coaxial cables, as in [5].

Future work on these LPI's needs to address the following:

- Incorporation of the proximity effect in a more direct manner into the analytical model.
- Improvement of the correlation between the measured and calculated phase responses.
- Realization of thicker inner line layers for the 50mm/1.5kA case.
- Determination of maximum noise/interference current as a percentage of nominal current, and it's relationship with attenuation response.
- Thermal issues. Heat due toe inner line dissipation is trapped within the outer lines. Ceramics utilised are extremely sensitive to thermal shock and heat concentration.
- Less brittle ceramics with the same dielectric properties. At present, manufacture and application of this technology is severly inhibted by this factor.

In conclusion. Integrated, planar, stacked LPI's, shorter than 0.15m, with 0dB attenuation at nominal power frequencies, and –40dB attenuation at 20MHz, were synthesized, modelled and built. These LPI's are for all practical purposes, invariant with load size. Application to widely varying cross-sectional dimensions has been proven. Incorporation into future integrated power electronics technology will require certain aspects, as outlined, to be adressed.

# 9 Literature:


[1] – J.D. van Wyk, F.C. Lee: "Power Electronics at the Dawn of the New Millenium – Status and Future", *IEEE PESC Conf. June 1999, Charleston, NC, USA, Proc., Vol. 1, p. 3 –12.*

[2] – H.M. Schlicke: "Assuredly Effective Filters", *IEEE Transactions on EMC, Vol. EMC –18, No. 3, August 1976.*

[3] – H. Zhu. A.R. Heffner, J.S. Lai: "Characterization of Power Electronics System Interconnect Parasitics using Time Domain Reflectometry", *IEEE PESC Conf. 1998, Proc., p. 1937 – 1943.*

[4] – F. Mayer: "RFI Suppresion Components: State of the Art, New Developments", *IEEE Transactions on EMC, Vol. EMC-18, No. 2, p. 59-70, May 1976.*

[5] – F. Mayer: "Improvements on the MIL-STD-85485 Low-Pass Cable Line", *IEEE EMC Symposium 1996, Proc., p.532 - 536.*

[6] – F. Mayer: "Electrical Power and Signal Distribution in Modern Aircrafts, Combines Weight Advantages and EMC Compatibility", *IEEE EMC Symposium, 1998, Proc., p. 281 - 283*

[7] – E.G. Cristal: "Parallel-coupled-line Filters Suitable for Microstrip and Stripline Realizations, Hairpin-Line Filters*", IEEE Transactions on Microwave Theory and Techniques, Nov. 1972, p.719 – 728.*

[8] – J. Huruya, R. Sato: "Transmission Characteristics and Design Method of Transmissionline Low-Pass Filters with Multiple Pairs on Coincident Zero's, and Multiple Pairs of Coincident Poles", *IEEE Transactions on Microwave Theory and Techniques, Aug, 1980, p. 865 874.*

[9] – J.D. van Wyk jr.: "Proposal Concerning Interconnect based Filters for CPES", *Internal Report, Industrial Electronics Research Group, Oct. 2001, Rand Afrikaans University, Johannesburg, South Africa.*
[10] – J.D. van Wyk jr.: "2nd Report on proposed Integrated Interconnect based Filters for CPES", *Internal Report, Industrial Electronics Research Group, Oct. 2001, Rand Afrikaans University, Johannesburg, South Africa.*
[11] – J.D. van Wyk jr.: "Reference Structures for some of the CPES proposed Integrated Interconnect based Filters", *Internal Report, Industrial Electronics Research Group, Nov. 2001, Rand Afrikaans University, Johannesburg, South Africa.*
[12] – R.A. Perala, K. Lee: "Induced Effects of Lightning on an All Composite Aircraft", *EMC Zurich Conf. Proc*., 1979, paper 79, p. 421 – 424.
[13] – J.D. Kraus, D.A. Fleisch: "Electromagnetics with Applications", Fifth Edition, McGraw-Hill, 1999.
[14] – R. Chipman: "Theory and Problems of Transmission Lines", Schaum's Outline Series, McGraw-Hill, New York, 1968
[15] – G. Brown, R.A. Sharpe, W.L. Hughes, R.E. Post: "Lines, Waves and Antennas, the Transmission of Electric Energy", 2nd Edition, John Wiley and Sons, 1973.
[16] – J.D. van Wyk jr., P.J. Wolmarans, J.D. van Wyk, W.A. Cronje: "Integrated RF-EMI Transmission Line Filters for Integrated Power Electronic Modules", Annual Seminar, Centre for Power Electronic Systems, Blacksburg, Virginia, USA, April 2002, Proceedings.
[17] – AnSoft Corporation: 2D FEM Field Solver Software, Version 3.0.21 , Materials Library



# 11 Appendix A:

Parametric Analysis Results

## 11.1 Design 17, Length: 0.01m, 0.05m and 0.5m.

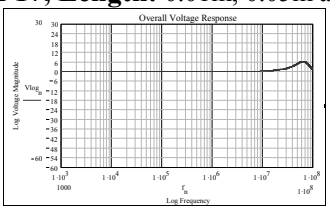


**Fig. A1:** Gain response for 0.01m of Design 17

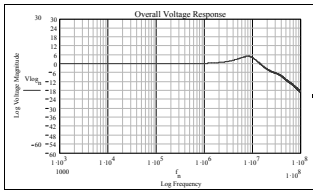


**Fig. A2:** Gain response for 0.05m of Design 17

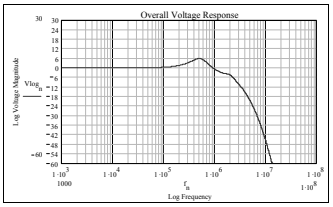


**Fig. A3:** Gain response for 0.5m of Design 17.

## 11.2 Design 17, Load Value: 20.01Ω, 0.1Ω, 0.5Ω, 5Ω - 1MΩ

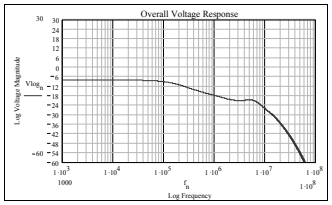


**Fig. A4:** Gain for Design 17 with 0.01Ω load.

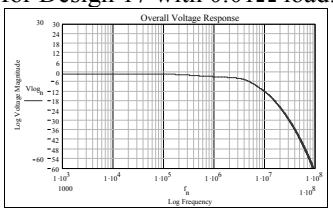


**Fig. A5:** Gain for Design 17 with 0.1Ω load.

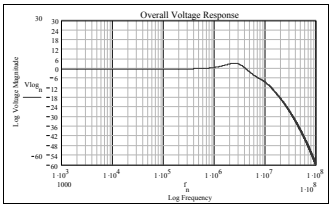


**Fig. A6:** Gain for Design 17 with 0.5Ω load.

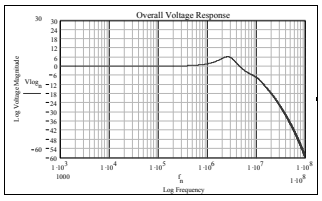


**Fig. A7:** Gain for Design 17 with 5Ω - 1MΩ load.

## 11.3 Design 17, Sigma of inner line: σ = 1e5, σ =1.6e6, σ = 5e7.

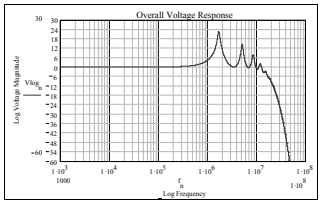


**Fig. A8:** Gain for Design 17, with σ = 1e5 S/m

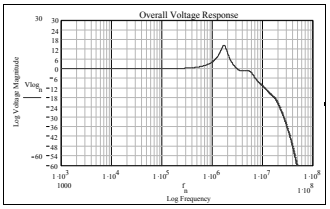


**Fig. A9:** Gain for Design 17, with $\sigma$ = 1e6 S/m

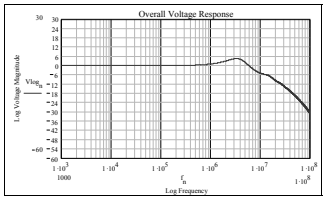


**Fig. A10:** Gain for Design 17, with $\sigma$ = 5e7 S/m

### 11.4 Design 17, Relative permeability of inner line: $\mu_r = 1$, $\mu_r = 25$, $\mu_r = 600$.

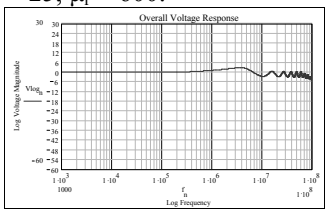


**Fig. A11:** Gain for Design 17, with $\mu_r = 1$

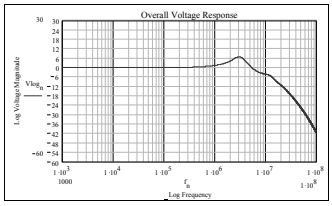


**Fig. A12:** Gain for Design 17, with $\mu_r = 25$.

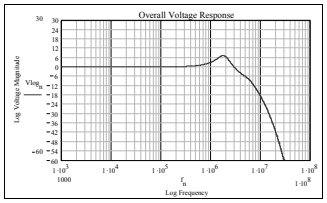


**Fig. A13:** Gain for Design 17, with $\mu_r$ =600.

### 11.5 Design 17, Relative permittivity of ceramic: $\varepsilon_r$ =500, $\varepsilon_r = 1000$, $\varepsilon_r = 20000$.

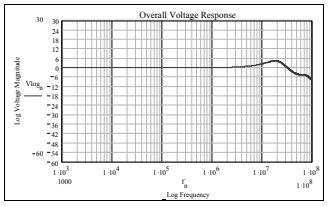


**Fig. A14:** Gain for Design 17 with $\varepsilon_r = 500$

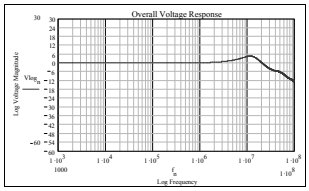


**Fig. A15:**Gain for Design 17 with $\varepsilon_r = 1000$.

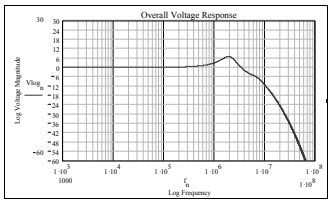


**Fig. A16:** Gain for Design 17 with $\varepsilon_r = 20000$

### 11.6 HC-Design 20, length of interconnect: l = 0.05m, l = 0.2m, l = 0.5m.

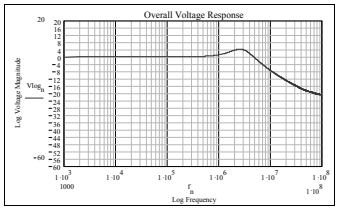


**Fig. A.17:** Gain for HC-Design 20 with l = 0.05m

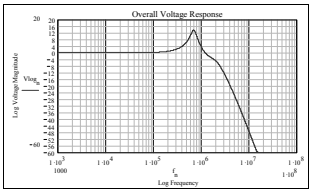


**Fig. A.18:** Gain for HC-Design 20 with l = 0.2m

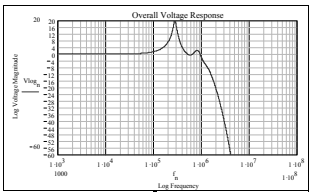


**Fig. A.19:** Gain for HC-Design 20 with l = 0.5m